Inorg. Chem. **2005**, *44*, 5081–5091

Metal–Metal Interactions in Mixed-Valence $[M_2Cl_9]^{2-}$ Species: Electronic Structure of d^1d^2 (V, Nb, Ta) and d^4d^5 (Fe, Ru, Os) Face-Shared Systems

Germán Cavigliasso and Robert Stranger*

Department of Chemistry, Faculty of Science, Australian National University, Canberra ACT 0200, Australia

Received February 1, 2005

The molecular and electronic structures of mixed-valence d^1d^2 (V, Nb, Ta) and d^4d^5 (Fe, Ru, Os) face-shared $[M_2Cl_9]^{2-}$ dimers have been calculated by density functional methods in order to investigate metal–metal bonding in this series. General similarities are observed between d^1d^2 and d^4d^5 systems and can be considered to reflect the electron–hole equivalence of the individual d^1–d^5 and d^2–d^4 configurations. The electronic structures of the dimers have been analyzed using potential energy curves for the broken-symmetry and other spin states resulting from the d^1d^2 and d^4d^5 coupling modes. In general, a spin-doublet ($S = 1/2$) state, characterized by delocalization of the metal-based electrons in a metal–metal bond with a formal order of 1.5, is favored in the systems containing 4d and 5d metals, namely, the Nb, Ta, Ru, and Os dimers. In contrast, the calculated ground structures for $[V_2Cl_9]^{2-}$ and $[Fe_2Cl_9]^{2-}$ correspond to a spin-quartet ($S = 3/2$) state involving weaker coupling between the metal centers and electron localization. In the case of $[Ru_2Cl_9]^{2-}$, both the spin-doublet and spin-quartet states are predicted to be energetically favored suggesting that this species may exhibit double-minima behavior. A comparison of computational results across the (d^1d^1, d^1d^2, d^2d^2) $[Nb_2Cl_9]^{z-}$ and $[Ta_2Cl_9]^{z-}$ and (d^4d^4, d^4d^5, d^5d^5) $[Ru_2Cl_9]^{z-}$ and $[Os_2Cl_9]^{z-}$ series has revealed that, in all four cases, the shortening of the metal–metal distances correlates with an increase in formal metal–metal bond order.

1. Introduction

The dinuclear compounds represented by the face-shared $[M_2X_9]^{z-}$ species (Figure 1) constitute an important class among the systems involving metal−metal interactions because they are formed by many transition metals and exhibit widely varied structural, electronic, and magnetic properties. These $[M_2X_9]^{z-}$ "dimers" are also attractive from a computational point of view because their relatively small size and high symmetry make them amenable to relatively high-level calculations.

The diversity of bonding possibilities makes the theoretical and computational treatment of the electronic structures of the $[M_2X_9]^{z-}$ dimers especially challenging. Nevertheless, we have shown in our previous publications[1−8] that density functional theory in combination with the broken-symmetry approach (developed by Noodleman and co-workers[9,10]) can accurately describe the entire range of metal−metal interactions, from weak antiferromagnetic coupling through to strong multiply bonded metal centers, as well as encompassing both high-spin and low-spin metal configurations.

Most of our previous work on face-shared $[M_2X_9]^{z-}$ species has focused on "even-electron" or "same-valence" systems, characterized by d^1d^1, d^2d^2, d^3d^3, d^4d^4, and d^5d^5 electronic configurations, but more recently, we have extended our investigations to d^2d^3 (Cr, Mo, W) and d^3d^4 (Mn, Tc, Re) mixed-valence dimers.[11] The general nature of the metal−metal interactions in the d^2d^3 and d^3d^4 mixed-valence species is similar to that found for their d^2d^2, d^3d^3, and d^4d^4

* To whom correspondence should be addressed. E-mail: rob.stranger@anu.edu.au.

(1) Lovell, T.; McGrady, J. E.; Stranger, R.; Macgregor, S. A. *Inorg. Chem.* **1996**, *35*, 3079.
(2) McGrady, J. E.; Stranger, R.; Lovell, T. *J. Phys. Chem. A* **1997**, *101*, 6265.
(3) Stranger, R.; McGrady, J. E.; Lovell, T. *Inorg. Chem.* **1998**, *37*, 6795.
(4) Lovell, T.; Stranger, R.; McGrady, J. E. *Inorg. Chem.* **2001**, *40*, 39.
(5) Stranger, R.; Turner, A.; Delfs, C. D. *Inorg. Chem.* **2001**, *40*, 4093.
(6) Petrie, S.; Stranger, R. *Polyhedron* **2002**, *21*, 1163.
(7) Stranger, R.; Lovell, T.; McGrady, J. E. *Polyhedron* **2002**, *21*, 1969.
(8) Cavigliasso, G.; Stranger, R. *Inorg. Chem.* **2004**, *43*, 2368.
(9) Noodleman, L.; Norman, J. G. *J. Chem. Phys.* **1979**, *70*, 4903.
(10) Noodleman, L. *J. Chem. Phys.* **1981**, *74*, 5737.
(11) Cavigliasso, G.; Comba, P.; Stranger, R. *Inorg. Chem.* **2004**, *43*, 6734.

10.1021/ic050175f CCC: $30.25
Published on Web 06/07/2005

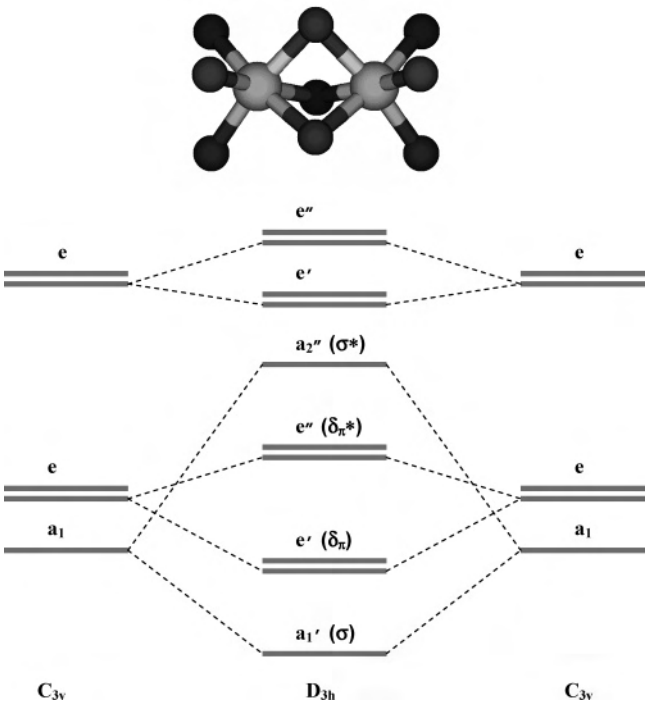

Figure 1. Schematic representation of the correlation between metal-based molecular orbitals in C_{3v} (broken-symmetry) and D_{3h} (full-symmetry) descriptions.

counterparts. Electron delocalization and metal−metal bonding play a dominant role in systems containing 4d and 5d elements, while electron localization and weaker coupling between the metal centers are favored in the dimers formed by 3d elements.

In this article, we further extend our computational studies of mixed-valence systems to species possessing d^1d^2 and d^4d^5 electronic configurations represented by the $[V_2Cl_9]^{2-}$, $[Nb_2Cl_9]^{2-}$, and $[Ta_2Cl_9]^{2-}$ and $[Fe_2Cl_9]^{2-}$, $[Ru_2Cl_9]^{2-}$, and $[Os_2Cl_9]^{2-}$ groups, respectively. The description and analysis of the electronic structures of these dimers were carried out by exploring the potential energy curves for the broken-symmetry and other spin states corresponding to several possible coupling modes of the metal centers.

This study of d^1d^2 and d^4d^5 dimers completes our investigations on the electronic structures and metal−metal interactions in face-shared $[M_2X_9]^{z-}$ species, and it also provides the necessary data to undertake an analysis of the periodic trends in metal−metal interactions across the entire series of face-shared $[M_2Cl_9]^{z-}$ species, which includes systems with even-electron (d^1d^1, d^2d^2, d^3d^3, d^4d^4, and d^5d^5) and odd-electron (d^1d^2, d^2d^3, d^3d^4, and d^4d^5) configurations and all of the transition elements from groups 4−8.

2. Calculation Details

All density functional calculations reported in this article were carried out with the ADF (2002.03) program.[12−14] Functionals based on the Volko−Wilk−Nusair[15] (VWN) form of the local-density approximation[16] (LDA) were utilized, and basis sets of triple-ζ quality and one polarization function (TZP or type IV), incorporating a frozen core (Cl.2p and M.2p, M.3d, and M.4f for the first, second, and third transition-metal series, respectively), were employed.[12−14]

Methods such as gradient or relativistic corrections were not used because previous work,[17] involving a set of 16 well-characterized dinuclear complexes exhibiting a variety of ligand environments and a range of metal−metal bond orders from 0 to 4, has shown that these corrections normally result in poorer agreement with experimental structural data in the case of multiply charged species.

Furthermore, our computational procedure (based on the LDA) has been able to satisfactorily reproduce a variety of experimentally observed properties not only for the most typical examples of face-shared $[M_2X_9]^{z-}$ dimers, represented by the d^3d^3 systems formed by Cr, Mo, and W, but also for species displaying more "complicated" electronic structures, such as the d^2d^2 (V and Nb), d^5d^5 (Ru), d^2d^3 (Cr, Mo, W), and d^3d^4 (Mn, Tc, Re) dimers.

Experimental information for the d^1d^2 (V, Nb, Ta) and d^4d^5 (Fe, Ru, Os) dimers studied in the present work is scarce, but on the basis of the success of our density functional methodology in reproducing experimental results for d^2d^3 $[W_2Cl_9]^{2-}$ and d^3d^4 $[Re_2Cl_9]^{2-}$ and observations across a series of both same- and mixed-valence W and Re dimers,[11] we are confident that the molecular structures and properties, in particular the metal−metal distances, of the d^1d^2 and d^4d^5 systems can also be satisfactorily predicted.

Calculations on the $[M_2Cl_9]^{2-}$ systems were carried out using full (D_{3h}) molecular symmetry, with the exception of the broken-symmetry calculations which employed C_{3v} symmetry. It should be noted that the primary goal of this work is the qualitative description and understanding of trends in metal−metal interactions in d^1d^2 and d^4d^5 species, and therefore, calculations were performed only on the broken-symmetry and other spin states considered to be most relevant to the analysis of the electronic structures of these systems but not on all of the possible states arising from the various d^1d^2 and d^4d^5 coupling modes.

3. Results and Discussion

We have shown in our previous publications[2−8,11] that a satisfactory description of the entire range of metal−metal interactions in face-shared $[M_2X_9]^{z-}$ dimers can be achieved with an approach based on the analysis of the broken-symmetry potential energy curves in terms of the curves for the associated spin states which occur when one or more subsets of metal-based electrons are engaged in metal−metal bonding.

This methodology has been successfully applied to many even-electron systems with metal-based electronic configurations ranging from d^1d^1 through d^5d^5 and also to the odd-electron or mixed-valence species represented by the d^2d^3 (Cr, Mo, W) and d^3d^4 (Mn, Tc, Re) dimers.

The molecular structure of face-shared $[M_2Cl_9]^{z-}$ dimers (Figure 1) exhibits ideal D_{3h} geometry. When symmetry breaking is imposed on this structure, the result is a

(12) *ADF*, version 2002.03; SCM, Theoretical Chemistry, Vrije Universiteit: Amsterdam, The Netherlands (http://www.scm.com).
(13) Fonseca Guerra, C.; Snijders, J. G.; te Velde, G.; Baerends, E. J. *Theor. Chem. Acc.* **1998**, *99*, 391.
(14) te Velde, G.; Bickelhaupt, F. M.; Baerends, E. J.; Fonseca Guerra, C.; van Gisbergen, S. J. A.; Snijders, J. G.; Ziegler, T. *J. Comput. Chem.* **2001**, *22*, 931.
(15) Vosko, S. H.; Wilk, L.; Nusair, M. *Can. J. Phys.* **1980**, *58*, 1200.
(16) Kohn, W.; Sham, L. J. *Phys. Rev.* **1965**, *140*, A1133.
(17) Petrie, S.; Stranger, R. *Inorg. Chem.* **2004**, *43*, 2597.

Table 1. Electronic Configurations and Multiplets Resulting from the Coupling Modes of d^1d^2 $[M_2Cl_9]^{2-}$ Systems

coupling mode	configuration	spin state	multiplets[a]
$[a_1 \times a_1e]$	$[(a_1'\uparrow)^1(a_1'\downarrow)^1(e'\uparrow)^1(e'\downarrow)^0(e''\uparrow)^0(e''\downarrow)^0(a_2''\uparrow)^0(a_2''\downarrow)^0]$	$S = 1/2$	$^2\mathbf{E}'$
	$[(a_1'\uparrow)^1(a_1'\downarrow)^0(e'\uparrow)^1(e'\downarrow)^0(e''\uparrow)^0(e''\downarrow)^0(a_2''\uparrow)^1(a_2''\downarrow)^0]$	$S = 3/2$	$^4\mathbf{E}''$
$[a_1 \times e^2]$	$[(a_1'\uparrow)^0(a_1'\downarrow)^1(e'\uparrow)^2(e'\downarrow)^0(e''\uparrow)^0(e''\downarrow)^0(a_2''\uparrow)^0(a_2''\downarrow)^0]$	$S = 1/2'$	$^2A_2'$
	$[(a_1'\uparrow)^1(a_1'\downarrow)^0(e'\uparrow)^2(e'\downarrow)^0(e''\uparrow)^0(e''\downarrow)^0(a_2''\uparrow)^0(a_2''\downarrow)^0]$	$S = 3/2'$	$^4\mathbf{A_2}'$
$[e \times a_1e]$	$[(a_1'\uparrow)^1(a_1'\downarrow)^0(e'\uparrow)^1(e'\downarrow)^1(e''\uparrow)^0(e''\downarrow)^0(a_2''\uparrow)^0(a_2''\downarrow)^0]$	$S = 1/2$	$^2A_1' + {}^2E'$
	$[(a_1'\uparrow)^1(a_1'\downarrow)^0(e'\uparrow)^1(e'\downarrow)^0(e''\uparrow)^1(e''\downarrow)^0(a_2''\uparrow)^0(a_2''\downarrow)^0]$	$S = 3/2$	$^4A_1'' + {}^4A_2'' + {}^4E''$
$[e \times e^2]$	$[(a_1'\uparrow)^0(a_1'\downarrow)^0(e'\uparrow)^2(e'\downarrow)^1(e''\uparrow)^0(e''\downarrow)^0(a_2''\uparrow)^0(a_2''\downarrow)^0]$	$S = 1/2$	$^2\mathbf{E}'$
	$[(a_1'\uparrow)^0(a_1'\downarrow)^0(e'\uparrow)^2(e'\downarrow)^0(e''\uparrow)^1(e''\downarrow)^0(a_2''\uparrow)^0(a_2''\downarrow)^0]$	$S = 3/2$	$^4\mathbf{E}''$

[a] The energy of the multiplets highlighted in bold type can be calculated using a single-determinant approach.

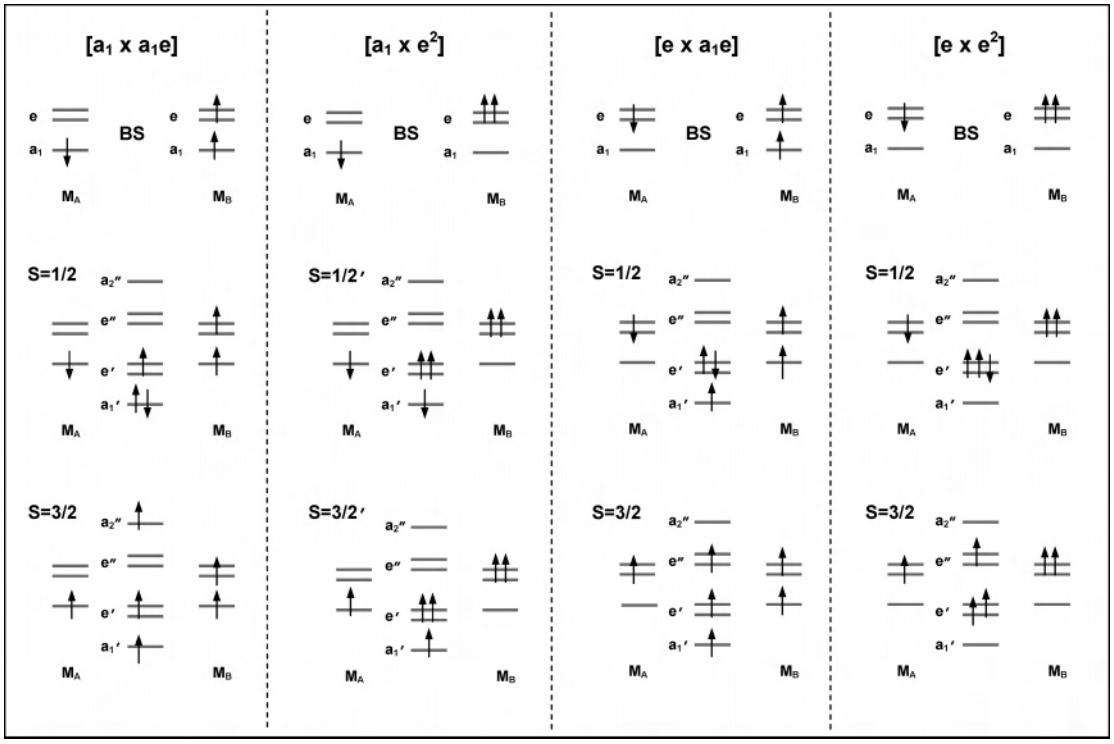

Figure 2. Schematic representation of the electronic configurations for the broken-symmetry and other spin states in the $[a_1 \times a_1e]$, $[e \times a_1e]$, $[a_1 \times e^2]$, and $[e \times e^2]$ coupling modes of d^1d^2 $[M_2Cl_9]^{2-}$ systems.

lowering of the molecular symmetry from D_{3h} to C_{3v} as a consequence of removing all of the symmetry elements connecting the metal centers. This procedure allows an asymmetric distribution of the unpaired spin density on opposite sides of the dimer and facilitates localization of the metal-based electrons when such a description is energetically favorable.

The correlation between C_{3v} and D_{3h} molecular orbital descriptions is shown in Figure 1. The connection between the (C_{3v}) broken-symmetry and (D_{3h}) associated states has been described in detail in previous publications[2−8,11] and results from the fact that when antiferromagnetic coupling within a subset of (σ and δ_π) electrons is weak, the corresponding ferromagnetic associated state, where the weakly coupled electrons are aligned in parallel, lies close in energy to the broken-symmetry state.

The local C_{3v} symmetry of the metal sites in the $[M_2X_9]^{z-}$ dimers splits the t_{2g} set of orbitals in an ideal octahedral ($[MX_6]^{z-}$) complex into a_1 and e subsets. In the most typical case, represented by d^3d^3 species, the "natural" occupancy of these levels corresponds to the $[(a_1)^1(e)^2]$ single-ion configuration and results in only one coupling mode. For d^1d^2 and d^4d^5 systems, however, several single-ion configurations are possible because of the different occupation patterns of the a_1 and e orbitals, resulting in a number of coupling modes.

The potential energy curves for the broken-symmetry and associated states corresponding to various d^1d^2 and d^4d^5 coupling modes are described in sections 3.1 and 3.2, respectively. The $[V_2Cl_9]^{2-}$ and $[Fe_2Cl_9]^{2-}$ dimers are analyzed in detail, and the results for the analogous Nb, Ta, Ru, and Os systems are also discussed.

3.1. Potential Energy Curves for d^1d^2 $[M_2Cl_9]^{2-}$ Systems. Four coupling modes, $[a_1 \times a_1e]$, $[a_1 \times e^2]$, $[e \times a_1e]$, and $[e \times e^2]$, are relevant to d^1d^2 $[M_2Cl_9]^{2-}$ dimers. These four modes result from the possibility of the single electron in the d^1 center residing in either the a_1 or e orbital, and the two electrons associated with the d^2 metal center can be accommodated by both the a_1 and e orbitals or exclusively by the e orbitals.

Schematic representations for the electronic configurations of the broken-symmetry and other spin states (Table 1) for

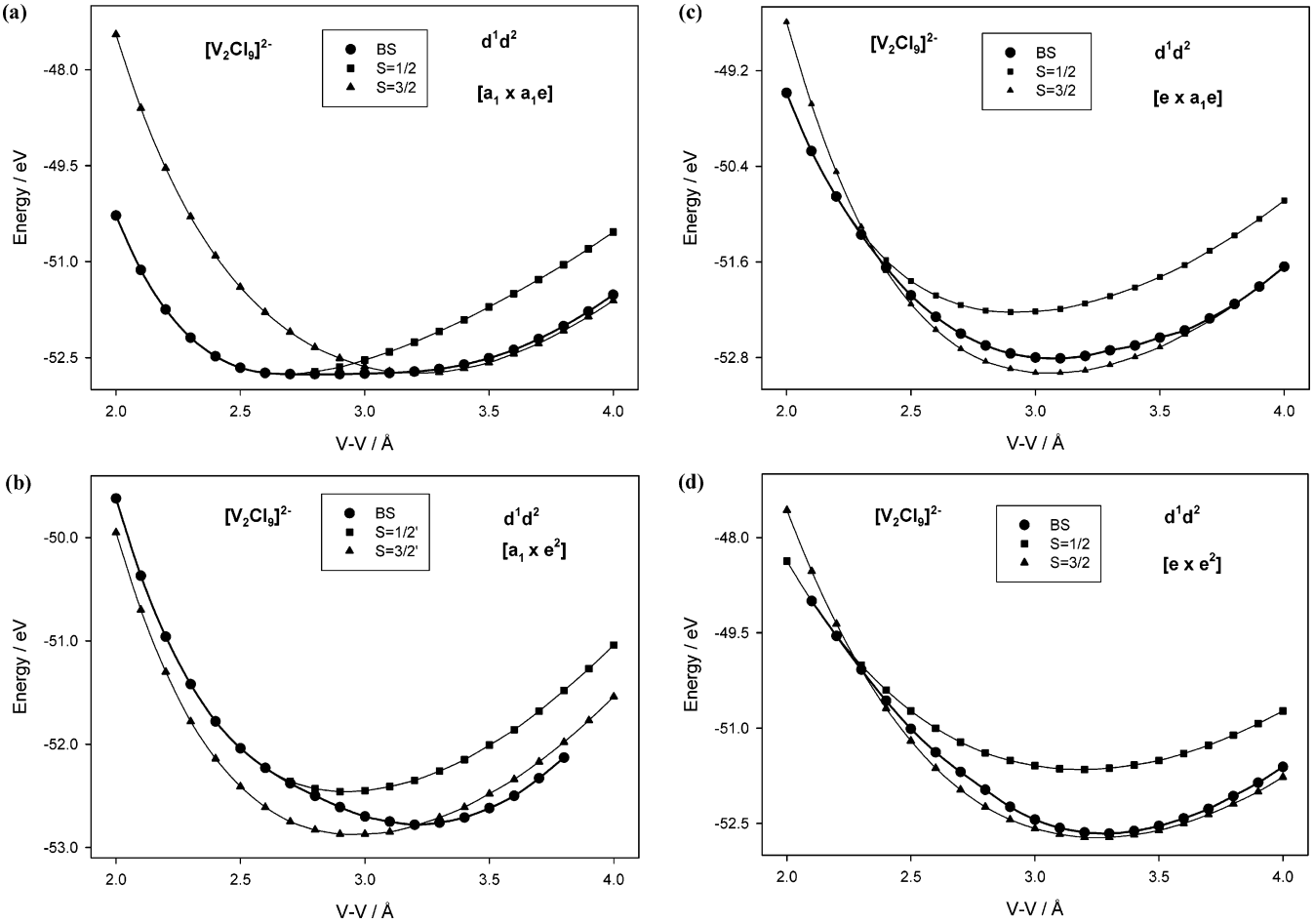

Figure 3. Potential energy curves for (d^1d^2) $[V_2Cl_9]^{2-}$.

all four coupling modes are given in Figure 2, and plots of the potential energy curves are shown in Figures 3 and 4. Optimized metal−metal distances and total bonding energies corresponding to the minima in the potential energy curves are summarized in Table 2.

3.1.1. Coupling Modes and Potential Energy Curves for $[V_2Cl_9]^{2-}$. In the $[a_1 \times a_1e]$ coupling mode, the broken-symmetry state corresponds to the $[(a_1\uparrow)^1(a_1\downarrow)^1(e\uparrow)^1(e\downarrow)^0(e\uparrow)^0(e\downarrow)^0(a_1\uparrow)^0(a_1\downarrow)^0]$ configuration. The potential energy curve for this broken-symmetry state can be discussed in terms of $S = 1/2$ and $S = 3/2$ associated states, which result from antiferromagnetic and ferromagnetic alignment of the σ electrons, respectively, with the single δ_π electron residing in the e′ orbitals.

Potential energy curves for the $[a_1 \times a_1e]$ broken-symmetry, $S = 1/2$, and $S = 3/2$ states are shown in section (a) of Figure 3. The broken-symmetry curve lies close to the $S = 3/2$ state at long metal−metal distances, indicating electron localization, whereas at short metal−metal distances, it converges with the $S = 1/2$ state in which electron delocalization occurs as a result of V−V bonding, characterized by a formal bond order of 1.5 corresponding to $[1.0\sigma + 0.5\delta_\pi]$. The results in Table 2 indicate that the energy difference between the $S = 1/2$ and $S = 3/2$ states is approximately 0.02 eV, and this is reflected in the flat nature of the broken-symmetry curve throughout the range of V−V separations connecting the $S = 1/2$ and $S = 3/2$ minima, which occur at 2.68 and 3.21 Å, respectively.

For the $[a_1 \times e^2]$ coupling mode, the broken-symmetry state is defined by the $[(a_1\uparrow)^0(a_1\downarrow)^1(e\uparrow)^2(e\downarrow)^0(e\uparrow)^0(e\downarrow)^0(a_1\uparrow)^0(a_1\downarrow)^0]$ configuration. In this case, the coupling between the d^1 and d^2 metal centers involves different subsets of electrons, and analogous to previous work,[3,8] the resulting doublet and quartet states are not described strictly as associated states and are labeled $S = 1/2'$ and $S = 3/2'$. Both states are characterized by a formal bond order of 1.5, corresponding to $[0.5\sigma + 1.0\delta_\pi]$, and have the same orbital occupation pattern, represented by $[(a_1')^1(e')^2]$, but with the relative alignment of the a_1' and e′ subsets of electrons being antiparallel in the $S = 1/2'$ state and parallel in the $S = 3/2'$ state.

Plots of the potential energy curves for the $[a_1 \times e^2]$ broken-symmetry, $S = 1/2'$, and $S = 3/2'$ states are given in section (b) of Figure 3. The $S = 1/2'$ and $S = 3/2'$ curves lie parallel to each other, with the latter at lower energy, throughout the entire range of metal−metal separations investigated. The broken-symmetry curve is almost coincident with the $S = 1/2'$ curve at V−V separations shorter than 2.6 Å but shifts to lower energy and lies closer to the $S = 3/2'$ curve at longer V−V distances. The global minimum for the $[a_1 \times e^2]$ coupling mode occurs at a metal−

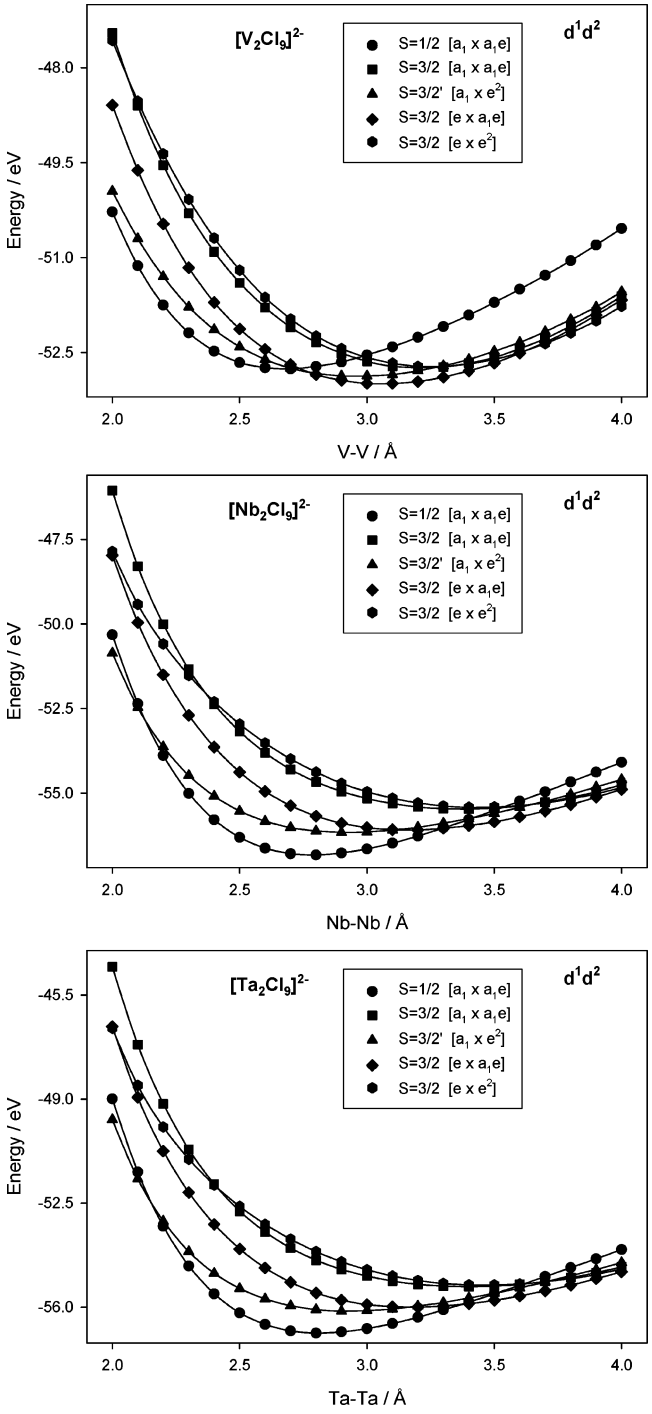

Figure 4. Potential energy curves for (d^1d^2) $[V_2Cl_9]^{2-}$, $[Nb_2Cl_9]^{2-}$, and $[Ta_2Cl_9]^{2-}$.

metal bond length of 2.96 Å and corresponds to the $S = 3/2'$ state.

The broken-symmetry state for the [e × a_1e] coupling mode is characterized by the $[(a_1\uparrow)^1(a_1\downarrow)^0(e\uparrow)^1(e\downarrow)^1(e\uparrow)^0(e\downarrow)^0(a_1\uparrow)^0(a_1\downarrow)^0]$ configuration and can be analyzed by considering $S = 1/2$ and $S = 3/2$ associated states, which correspond to antiferromagnetic and ferromagnetic alignment of the δ_π electrons, respectively, with the single σ electron occupying the a_1' orbital.

The potential energy curves for the [e × a_1e] broken-symmetry, $S = 1/2$, and $S = 3/2$ states are plotted in section (c) of Figure 3. The broken-symmetry curve coincides with the $S = 1/2$ curve at the shortest metal−metal separations investigated, where the V−V interaction is characterized by electron delocalization and formation of metal−metal bonds with a formal bond order of 1.5 corresponding to $[0.5\sigma + 1.0\delta_\pi]$, but is at a lower energy and closer to the $S = 3/2$ curve at all V−V distances longer than 2.4 Å.

Table 2. Optimized Metal−Metal Bond Distances (M−M in Å) and Total Bonding Energies (E_B in eV) for the Broken-Symmetry and Other Spin States Belonging to the [a_1 × a_1e], [a_1 × e^2], [e × a_1e], and [e × e^2] Coupling Modes of (d^1d^2) $[V_2Cl_9]^{2-}$, $[Nb_2Cl_9]^{2-}$, and $[Ta_2Cl_9]^{2-}$

molecule	coupling mode	state	M−M	E_B
$[V_2Cl_9]^{2-}$	[a_1 × a_1e]	BS	3.035	−52.76
		$S = 1/2$	2.679	−52.76
		$S = 3/2$	3.209	−52.74
	[a_1 × e^2]	BS	3.215	−52.79
		$S = 1/2'$	2.913	−52.46
		$S = 3/2'$	2.956	−52.88
	[e × a_1e]	BS	3.054	−52.81
		$S = 1/2$	2.915	−52.23
		$S = 3/2$	3.042	−53.00
	[e × e^2]	BS	3.278	−52.68
		$S = 1/2$	3.201	−51.65
		$S = 3/2$	3.254	−52.72
$[Nb_2Cl_9]^{2-}$	[a_1 × a_1e]	BS	2.786	−56.83
		$S = 1/2$	2.786	−56.83
		$S = 3/2$	3.379	−55.47
	[a_1 × e^2]	BS	3.282	−55.98
		$S = 1/2'$	2.913	−55.92
		$S = 3/2'$	2.921	−56.17
	[e × a_1e]	BS	3.181	−55.97
		$S = 1/2$	2.909	−55.79
		$S = 3/2$	3.144	−56.09
	[e × e^2]	BS	3.532	−55.64
		$S = 1/2$	3.276	−54.66
		$S = 3/2$	3.433	−55.42
$[Ta_2Cl_9]^{2-}$	[a_1 × a_1e]	BS	2.814	−56.87
		$S = 1/2$	2.820	−56.87
		$S = 3/2$	3.409	−55.31
	[a_1 × e^2]	BS	2.900	−55.90
		$S = 1/2'$	2.929	−55.90
		$S = 3/2'$	2.927	−56.13
	[e × a_1e]	BS	3.182	−55.88
		$S = 1/2$	2.926	−55.78
		$S = 3/2$	3.182	−56.00
	[e × e^2]	BS	3.564	−55.52
		$S = 1/2$	3.224	−54.57
		$S = 3/2$	3.457	−55.25

In addition to the $S = 3/2$ associated state, it is possible to define a delocalized quartet state for the [e × a_1e] coupling mode which corresponds exactly to the $S = 3/2'$ state described for the [a_1 × e^2] coupling mode. However, as shown by the results in Table 2, the associated $S = 3/2$ state is predicted to have a lower energy than the delocalized $S = 3/2'$ state and represents the [e × a_1e] global minimum at a V−V distance of 3.04 Å.

In the [e × e^2] coupling mode, the broken-symmetry state corresponds to the $[(a_1\uparrow)^0(a_1\downarrow)^0(e\uparrow)^2(e\downarrow)^1(e\uparrow)^0(e\downarrow)^0(a_1\uparrow)^0(a_1\downarrow)^0]$ configuration, and the $S = 1/2$ and $S = 3/2$ associated states can be defined by considering antiferromagnetic and ferromagnetic alignment patterns for the δ_π electrons, respectively.

Plots of the potential energy curves for the [e × e^2] broken-symmetry, $S = 1/2$, and $S = 3/2$ states are shown in section (d) of Figure 3. The broken-symmetry curve lies close to the $S = 3/2$ curve at all metal−metal distances greater than 2.2 Å but converges with the $S = 1/2$ curve at shorter metal−

Table 3. Electronic Configurations and Multiplets Resulting from the Coupling Modes of d^4d^5 $[M_2Cl_9]^{2-}$ Systems

coupling mode	configuration	spin state	multiplets[a]
$[a_1e^3 \times a_1e^4]$	$[(a_1'\uparrow)^1(a_1'\downarrow)^1(e''\uparrow)^2(e'\downarrow)^2(e''\uparrow)^2(e''\downarrow)^1(a_2''\uparrow)^0(a_2''\downarrow)^0]$	$S = 1/2$	$^2\mathbf{E}''$
	$[(a_1'\uparrow)^1(a_1'\downarrow)^0(e'\uparrow)^2(e'\downarrow)^2(e''\uparrow)^2(e''\downarrow)^1(a_2''\uparrow)^1(a_2''\downarrow)^0]$	$S = 3/2$	$^4\mathbf{E}'$
	$[(a_1'\uparrow)^1(a_1'\downarrow)^0(e'\uparrow)^2(e'\downarrow)^0(e''\uparrow)^2(e''\downarrow)^0(a_2''\uparrow)^1(a_2''\downarrow)^0(e'\uparrow)^2(e'\downarrow)^0(e''\uparrow)^1(e''\downarrow)^0]$	$S = 9/2$	$^{10}\mathbf{E}'$
$[a_1e^3 \times a_1^2e^3]$	$[(a_1'\uparrow)^1(a_1'\downarrow)^1(e'\uparrow)^2(e'\downarrow)^2(e''\uparrow)^1(e''\downarrow)^1(a_2''\uparrow)^1(a_2''\downarrow)^0]$	$S = 1/2$	$^2A_2'' + {}^2E''$
	$[(a_1'\uparrow)^1(a_1'\downarrow)^1(e'\uparrow)^2(e'\downarrow)^1(e''\uparrow)^2(e''\downarrow)^1(a_2''\uparrow)^1(a_2''\downarrow)^0]$	$S = 3/2$	$^4A_1' + {}^4A_2' + {}^4E'$
	$[(a_1'\uparrow)^1(a_1'\downarrow)^1(e'\uparrow)^2(e'\downarrow)^0(e''\uparrow)^2(e''\downarrow)^0(a_2''\uparrow)^1(a_2''\downarrow)^0(e'\uparrow)^2(e'\downarrow)^0(e''\uparrow)^0(e''\downarrow)^0]$	$S = 7/2$	$^8\mathbf{A_1}''$
$[a_1^2e^2 \times a_1e^4]$	$[(a_1'\uparrow)^1(a_1'\downarrow)^1(e'\uparrow)^2(e'\downarrow)^2(e''\uparrow)^2(e''\downarrow)^0(a_2''\uparrow)^0(a_2''\downarrow)^1]$	$S = 1/2'$	$^2A_1''$
	$[(a_1'\uparrow)^1(a_1'\downarrow)^1(e'\uparrow)^2(e'\downarrow)^2(e''\uparrow)^2(e''\downarrow)^0(a_2''\uparrow)^1(a_2''\downarrow)^0]$	$S = 3/2'$	$^4\mathbf{A_1}''$
$[a_1^2e^2 \times a_1^2e^3]$	$[(a_1'\uparrow)^1(a_1'\downarrow)^1(e'\uparrow)^2(e'\downarrow)^2(e''\uparrow)^1(e''\downarrow)^0(a_2''\uparrow)^1(a_2''\downarrow)^1]$	$S = 1/2$	$^2\mathbf{E}''$
	$[(a_1'\uparrow)^1(a_1'\downarrow)^1(e'\uparrow)^2(e'\downarrow)^1(e''\uparrow)^2(e''\downarrow)^0(a_2''\uparrow)^1(a_2''\downarrow)^1]$	$S = 3/2$	$^4\mathbf{E}'$
	$[(a_1'\uparrow)^1(a_1'\downarrow)^1(e'\uparrow)^2(e'\downarrow)^0(e''\uparrow)^2(e''\downarrow)^0(a_2''\uparrow)^1(a_2''\downarrow)^1(e'\uparrow)^1(e'\downarrow)^0(e''\uparrow)^0(e''\downarrow)^0]$	$S = 5/2$	$^6\mathbf{E}'$

[a] The energy of the multiplets highlighted in bold type can be calculated using a single-determinant approach.

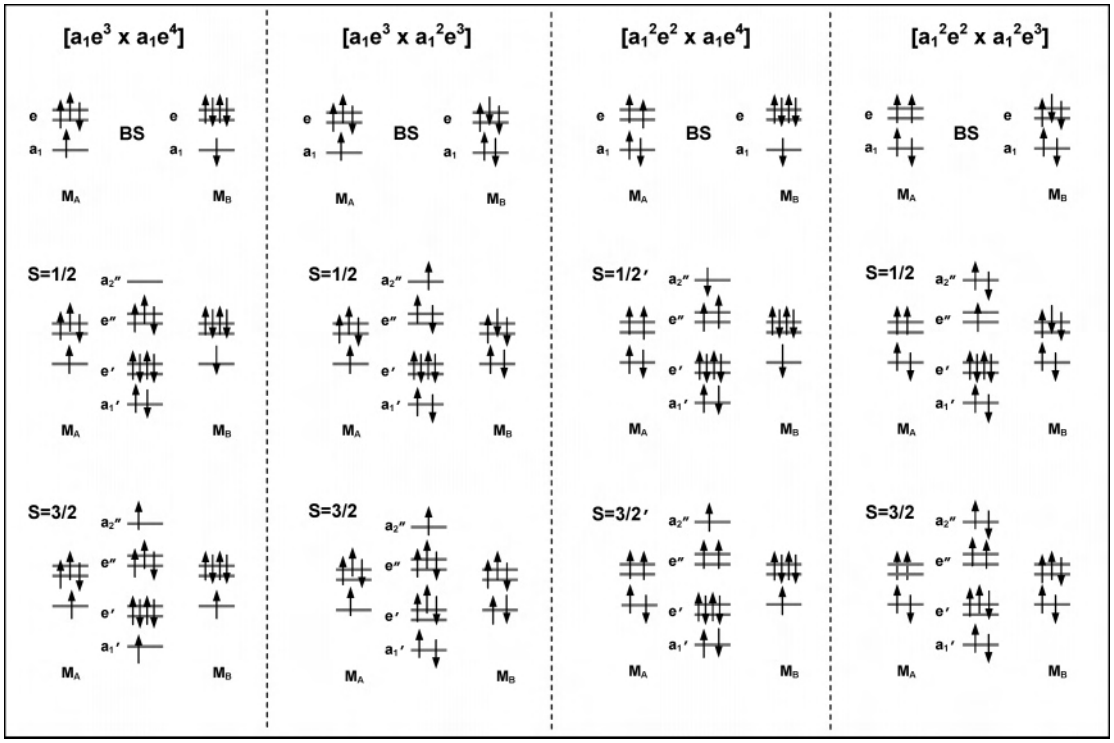

Figure 5. Schematic representation of the electronic configurations for the broken-symmetry and other spin states in the $[a_1e^3 \times a_1e^4]$, $[a_1e^3 \times a_1^2e^3]$, $[a_1^2e^2 \times a_1e^4]$, and $[a_1^2e^2 \times a_1^2e^3]$ coupling modes of (d^4d^5) $[M_2Cl_9]^{2-}$ systems.

metal separations. The minimum for the $S = 3/2$ state, at a V−V distance of 3.25 Å, is close to that of the broken-symmetry curve and energetically lower than the minimum for the $S = 1/2$ state, indicating that localization of the metal-based electrons is favored for this coupling mode.

3.1.2. General Analysis of the Potential Energy Curves. The potential energy curves for the states that are most important for determining the global minima of $[V_2Cl_9]^{2-}$, $[Nb_2Cl_9]^{2-}$, and $[Ta_2Cl_9]^{2-}$ and for a comparative discussion of the most significant similarities and differences are collected in Figure 4.

For $[V_2Cl_9]^{2-}$, the quartet states from all four coupling modes are energetically favored at long metal−metal separations, whereas the $[a_1 \times a_1e]$ $S = 1/2$ state represents the lowest-lying potential energy curve at V−V distances shorter than 2.7 Å. The global minimum is predicted to occur at a V−V bond length of 3.04 Å and corresponds to the $S = 3/2$ state from the $[e \times a_1e]$ coupling mode.

In contrast, the global minimum for both $[Nb_2Cl_9]^{2-}$ and $[Ta_2Cl_9]^{2-}$ occurs at the relatively shorter metal−metal separations of 2.79 and 2.82 Å, respectively, and corresponds to the $S = 1/2$ state from the $[a_1 \times a_1e]$ coupling mode. The metal−metal interaction is characterized by electron delocalization in a Nb−Nb or Ta−Ta bond and a formal bond order of 1.5 corresponding to $[1.0\sigma + 0.5\delta_\pi]$. This state is clearly favored at metal−metal distances within the 2.2−3.2 Å range but shifts to higher energy at longer Nb−Nb or Ta−Ta separations where the $[e \times a_1e]$ $S = 3/2$ state represents the lowest-lying curve. As the metal−metal bond length increases beyond 3.6−3.7 Å, all four quartet states become energetically more favorable than the $[a_1 \times a_1e]$ $S = 1/2$ state.

3.2. Potential Energy Curves for d^4d^5 $[M_2Cl_9]^{2-}$ Systems. The description of the coupling modes and broken-symmetry and associated states for d^4d^5 $[M_2Cl_9]^{2-}$ dimers is analogous to that presented for d^1d^2 systems because the d^4 and d^5 configurations can be considered as the "hole" equivalents of the d^2 and d^1 configurations, respectively. The four coupling modes for d^4d^5 dimers are denoted $[a_1e^3 \times a_1e^4]$, $[a_1e^3 \times a_1^2e^3]$, $[a_1^2e^2 \times a_1e^4]$, and $[a_1^2e^2 \times a_1^2e^3]$ and

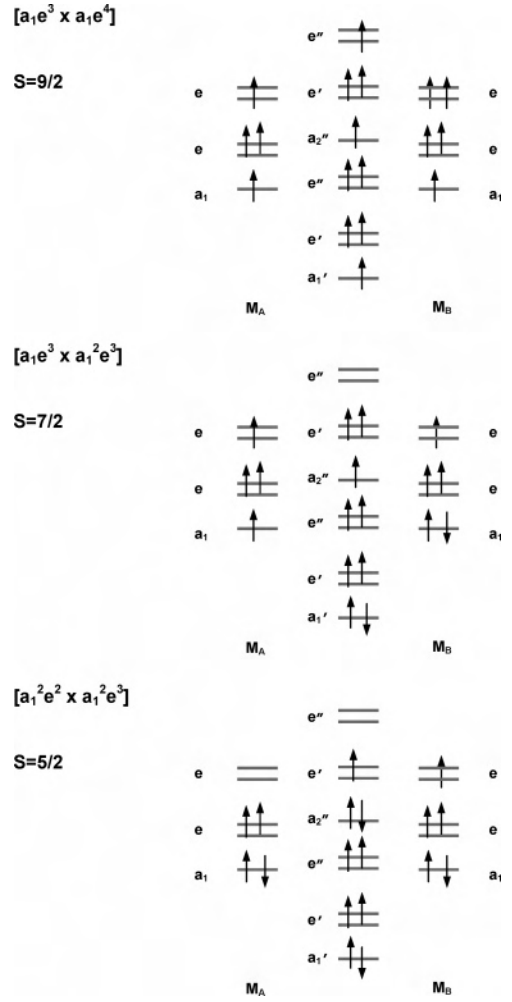

Figure 6. Schematic representation of the electronic configuration for the ($[a_1e^3 \times a_1e^4]$) $S = 9/2$, ($[a_1e^3 \times a_1^2e^3]$) $S = 7/2$, and ($[a_1^2e^2 \times a_1^2e^3]$) $S = 5/2$ states of (d^4d^5) $[M_2Cl_9]^{2-}$ systems.

correspond to the single-electron hole in the d^5 center being accommodated in either an a_1 or e orbital and the two electron holes associated with the d^4 metal center residing exclusively in the e orbitals or in both a_1 and e orbitals.

As in the d^1d^2 systems, broken-symmetry and spin-doublet and spin-quartet states (Table 3) can be defined for each of the four d^4d^5 coupling modes, and schematic representations of the respective electronic configurations are given in Figure 5. In addition, states resulting from the coupling of metal sites with high-spin d^4 and d^5 configurations also have to be considered in the analysis of the metal−metal interactions of $[Fe_2Cl_9]^{2-}$ (Table 3). The electronic configurations for these high-spin states are described in Figure 6.

Plots of the potential energy curves are shown in Figures 7 and 8, and optimized metal−metal distances and total bonding energies, corresponding to the minima in the potential energy curves, for the broken-symmetry and other spin states of the four d^4d^5 coupling modes are summarized in Table 4.

3.2.1. Coupling Modes and Potential Energy Curves for $[Fe_2Cl_9]^{2-}$. In the $[a_1e^3 \times a_1e^4]$ coupling mode, the broken-symmetry state corresponds to the $[(a_1\uparrow)^1(a_1\downarrow)^1(e\uparrow)^2(e\downarrow)^2(e\uparrow)^2(e\downarrow)^1(a_1\uparrow)^0(a_1\downarrow)^0]$ configuration. The potential energy curve for this broken-symmetry state can be discussed in terms of the $S = 1/2$, $S = 3/2$, and $S = 9/2$ associated states. The doublet and quartet states (Figure 5) correspond to antiferromagnetic and ferromagnetic alignment of the σ electrons, respectively, with the unpaired δ_π electron residing in the e orbitals, whereas the $S = 9/2$ state (Figure 6) results from the coupling of the metal centers with high-spin configurations.

Table 4. Optimized Metal−Metal Bond Distances (M−M in Å) and Total Bonding Energies (E_B in eV) for the Broken-Symmetry and Other Spin States Belonging to the $[a_1e^3 \times a_1e^4]$, $[a_1e^3 \times a_1^2e^3]$, $[a_1^2e^2 \times a_1e^4]$, and $[a_1^2e^2 \times a_1^2e^3]$ Coupling Modes of (d^4d^5) $[Fe_2Cl_9]^{2-}$, $[Ru_2Cl_9]^{2-}$, and $[Os_2Cl_9]^{2-}$

molecule	coupling mode	state	M−M	E_B
$[Fe_2Cl_9]^{2-}$	$[a_1e^3 \times a_1e^4]$	BS	3.316	−49.26
		$S = 1/2$	2.587	−48.53
		$S = 3/2$	2.999	−49.06
		$S = 9/2$	3.386	−49.18
	$[a_1e^3 \times a_1^2e^3]$	BS	2.877	−49.11
		$S = 1/2$	2.807	−48.54
		$S = 3/2$	2.877	−49.31
		$S = 7/2$	3.193	−48.74
	$[a_1^2e^2 \times a_1e^4]$	BS	3.035	−49.13
		$S = 1/2'$	2.810	−48.68
		$S = 3/2'$	2.781	−49.20
	$[a_1^2e^2 \times a_1^2e^3]$	BS	3.035	−49.05
		$S = 1/2$	2.983	−48.17
		$S = 3/2$	3.012	−49.08
		$S = 5/2$	3.171	−48.60
$[Ru_2Cl_9]^{2-}$	$[a_1e^3 \times a_1e^4]$	BS	2.645	−48.31
		$S = 1/2$	2.645	−48.31
		$S = 3/2$	3.138	−47.79
	$[a_1e^3 \times a_1^2e^3]$	BS	3.009	−48.19
		$S = 1/2$	2.815	−47.83
		$S = 3/2$	2.956	−48.28
	$[a_1^2e^2 \times a_1e^4]$	BS	3.050	−48.22
		$S = 1/2'$	2.808	−47.92
		$S = 3/2'$	2.804	−48.19
	$[a_1^2e^2 \times a_1^2e^3]$	BS	3.219	−47.99
		$S = 1/2$	3.068	−47.19
		$S = 3/2$	3.162	−47.83
$[Os_2Cl_9]^{2-}$	$[a_1e^3 \times a_1e^4]$	BS	2.701	−53.26
		$S = 1/2$	2.706	−53.26
		$S = 3/2$	3.230	−52.48
	$[a_1e^3 \times a_1^2e^3]$	BS	3.084	−52.99
		$S = 1/2$	2.856	−52.67
		$S = 3/2$	3.015	−53.05
	$[a_1^2e^2 \times a_1e^4]$	BS	3.110	−53.04
		$S = 1/2'$	2.851	−52.75
		$S = 3/2'$	2.842	−52.99
	$[a_1^2e^2 \times a_1^2e^3]$	BS	3.302	−52.77
		$S = 1/2$	3.126	−51.93
		$S = 3/2$	3.242	−52.53

It should be noted that the $S = 1/2$, $S = 3/2$, and $S = 9/2$ states can all be connected with the same $[a_1e^3 \times a_1e^4]$ broken-symmetry configuration because both e′ and e″ (D_{3h}) orbitals transform as the e (C_{3v}) irreducible representation when the molecular symmetry is reduced from D_{3h} to C_{3v}. This broken-symmetry configuration is characterized by an overall electron distribution corresponding to an $[(a_1)^2(e)^4(e)^3]$ orbital occupancy and can therefore encompass the description of both low-spin and high-spin cases.

Potential energy curves for the $[a_1e^3 \times a_1e^4]$ broken-symmetry, $S = 1/2$, $S = 3/2$, and $S = 9/2$ states are shown in section (a) of Figure 7. The broken-symmetry curve converges with the $S = 1/2$ state at short metal−metal distances, where electron delocalization occurs as a result of the formation of Fe−Fe bonds, characterized by a formal

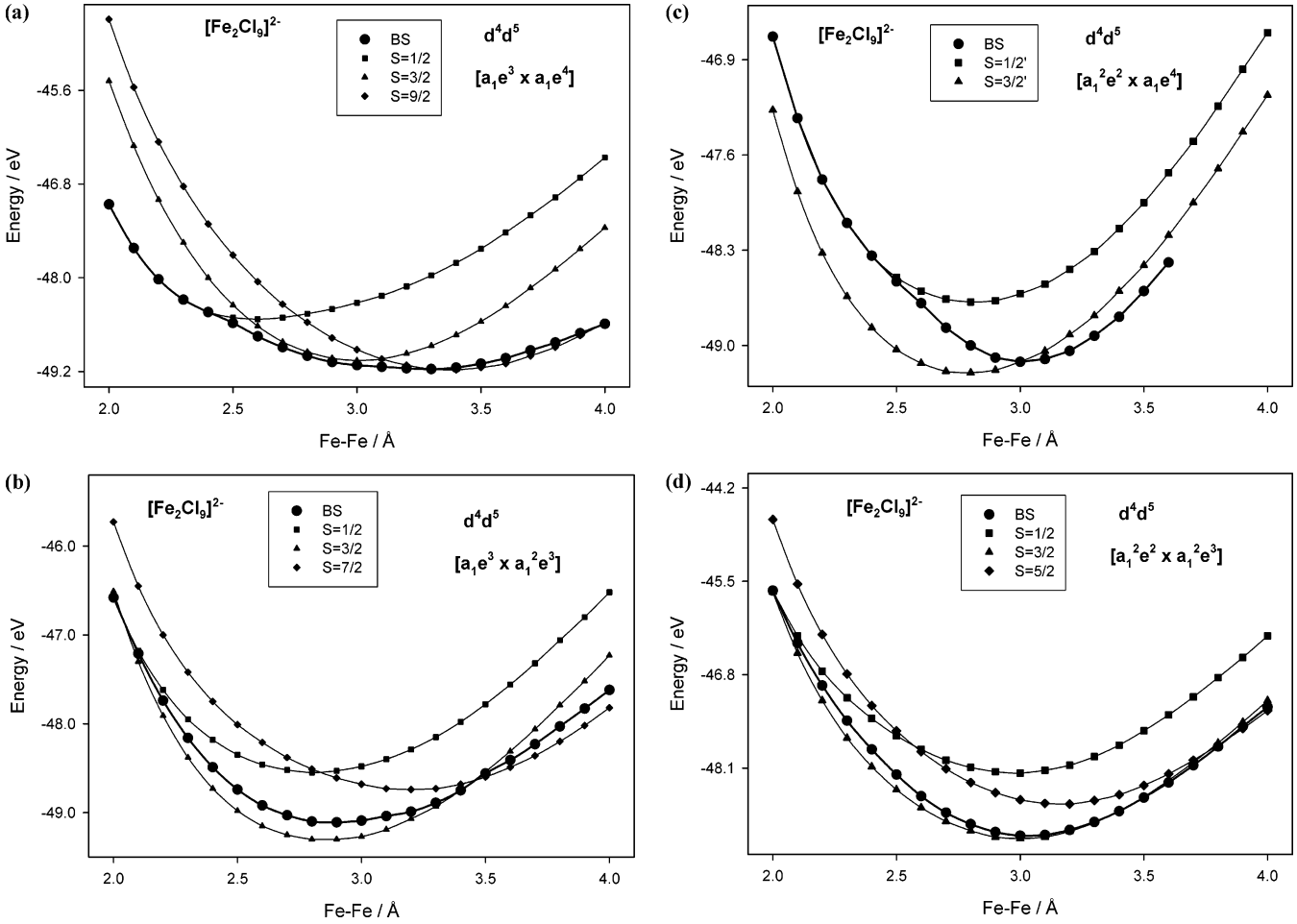

Figure 7. Potential energy curves for (d^4d^5) $[Fe_2Cl_9]^{2-}$.

bond order of 1.5 corresponding to $[1.0\sigma + 0.5\delta_\pi]$. However, as the Fe−Fe separation increases, the $S = 1/2$ curve shifts to higher energy, and the broken-symmetry curve lies close to the $S = 3/2$ state in the intermediate range of metal−metal distances, from approximately 2.6 to 3.0 Å, and to the $S = 9/2$ state at Fe−Fe separations longer than 3.1 Å. The global minimum occurs at a long metal−metal bond length of 3.3−3.4 Å where the $S = 9/2$ state is energetically favored, suggesting a preference for electron localization and high-spin configurations for this coupling mode.

The broken-symmetry state for the $[a_1e^3 \times a_1{}^2e^3]$ coupling mode is characterized by the $[(a_1\uparrow)^1(a_1\downarrow)^1(e\uparrow)^2(e\downarrow)^2(e\uparrow)^1(e\downarrow)^1(a_1\uparrow)^1(a_1\downarrow)^0]$ configuration and can be analyzed by considering the $S = 1/2$, $S = 3/2$, and $S = 7/2$ associated states, with the latter corresponding to the coupling of high-spin d^4 and d^5 metal sites (Figure 6) and the doublet and quartet states resulting from the antiferromagnetic and ferromagnetic alignment of the δ_π electrons (Figure 5), respectively, with the unpaired σ electron occupying the a_2'' orbital.

As discussed for the $[a_1e^3 \times a_1e^4]$ coupling mode, the symmetry properties of the δ_π orbitals in the D_{3h} and C_{3v} point groups imply that the low-spin and high-spin cases for the $[a_1e^3 \times a_1{}^2e^3]$ coupling mode can both be described by the same broken-symmetry configuration corresponding to an $[(a_1)^2(e)^4(e)^2(a_1)^1]$ orbital occupancy.

Plots of the potential energy curves for the $[a_1e^3 \times a_1{}^2e^3]$ broken-symmetry, $S = 1/2$, $S = 3/2$, and $S = 7/2$ states are given in section (b) of Figure 7. The quartet state is favored at most metal−metal separations, with the $S = 3/2$ curve lying closer to the broken-symmetry state than the $S = 1/2$ and $S = 7/2$ curves throughout the 2.1−3.4 Å range and represents the global minimum for this coupling mode at an Fe−Fe bond length of 2.88 Å. The metal−metal interaction at this minimum can be described as involving some degree of σ bonding, corresponding to a formal bond order of 0.5, but with a preference for localization of the unpaired δ_π electrons. The $S = 1/2$ and $S = 7/2$ states play significant roles only at the shortest and longest Fe−Fe distances investigated, respectively.

For the $[a_1{}^2e^2 \times a_1e^4]$ coupling mode, the broken-symmetry state is defined by the $[(a_1\uparrow)^1(a_1\downarrow)^1(e\uparrow)^2(e\downarrow)^2(e\uparrow)^1(e\downarrow)^1(a_1\uparrow)^0(a_1\downarrow)^1]$ configuration, and analogous to the $[a_1 \times e^2]$ mode of d^1d^2 systems, the coupling between the d^4 and d^5 metal centers involves different subsets of electrons. Therefore, the doublet and quartet states are not described strictly as associated states and are labeled $S = 1/2'$and $S = 3/2'$. These two states are characterized by the same overall orbital occupancy, represented by $[(a_1')^2(e')^4(e'')^2\ (a_2'')^1]$, and a formal metal−metal bond order of 1.5, corresponding to $[0.5\sigma + 1.0\delta_\pi]$,

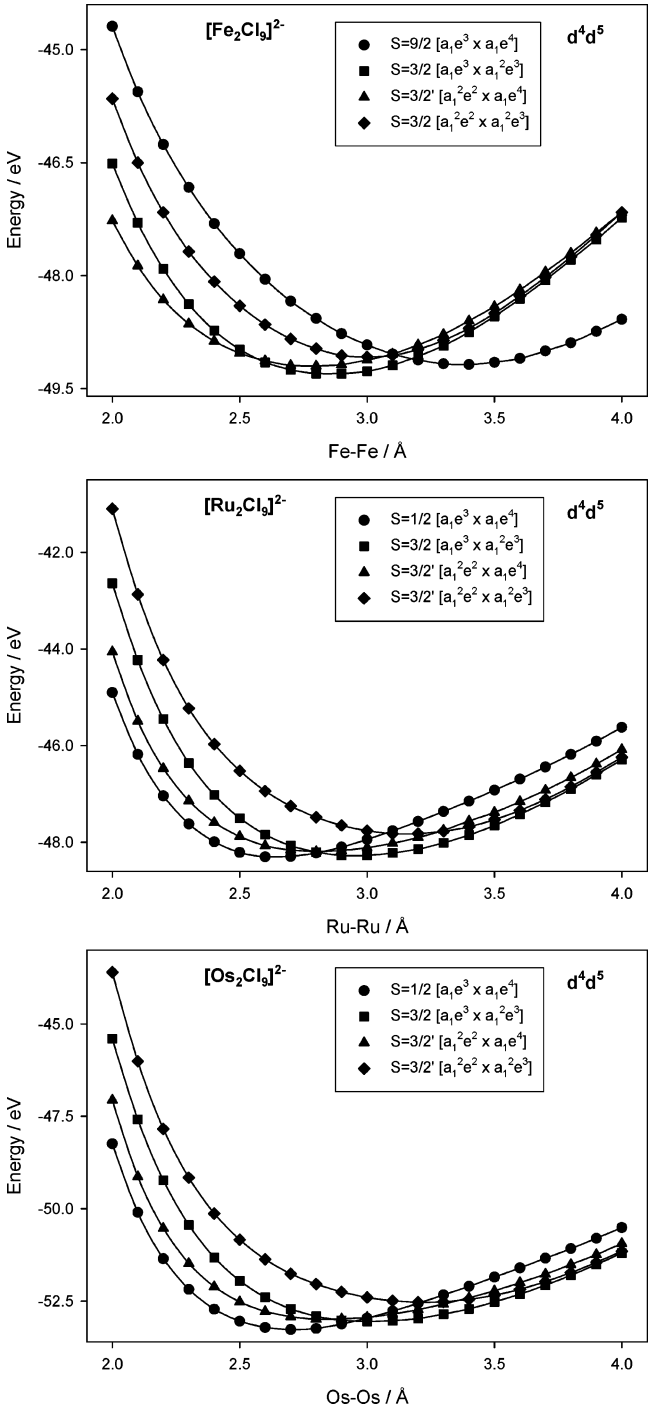

Figure 8. Potential energy curves for (d^4d^5) $[Fe_2Cl_9]^{2-}$, $[Ru_2Cl_9]^{2-}$, and $[Os_2Cl_9]^{2-}$.

but the relative alignment of the e″ and a_2″ subsets of electrons is antiparallel in the former and parallel in the latter.

The potential energy curves for the $[a_1^2e^2 \times a_1e^4]$ broken-symmetry, $S = 1/2'$, and $S = 3/2'$ states are plotted in section (c) of Figure 7. The behavior of the three curves is similar to that observed for the analogous $[a_1 \times e^2]$ coupling mode of the d^1d^2 V dimer. The $S = 1/2'$ and $S = 3/2'$curves lie parallel to each other throughout the entire range of metal−metal separations investigated at the quartet state, with a lower energy and representing the global minimum at an Fe−Fe distance of 2.78 Å. The broken-symmetry curve is almost coincident with the $S = 1/2'$ curve at metal−metal separations shorter than 2.6 Å but shifts to lower energy and lies closer to the $S = 3/2'$ curve at longer Fe−Fe distances.

It should be noted that the delocalized $S = 3/2'$ state can also be produced by the coupling pattern characteristic of the $[a_1e^3 \times a_1^2e^3]$ mode (Figure 5). However, it has not been explicitly considered in the description and analysis of the potential energy curves for this coupling mode because it is not an associated state and, as shown in Table 4, is predicted to have a higher energy than the $[a_1e^3 \times a_1^2e^3]$ $S = 3/2$ state.

In the $[a_1^2e^2 \times a_1^2e^3]$ coupling mode, the broken-symmetry curve is described by the $[(a_1\uparrow)^1(a_1\downarrow)^1(e\uparrow)^2(e\downarrow)^2(e\uparrow)^1(e\downarrow)^0(a_1\uparrow)^1(a_1\downarrow)^1]$ configuration and can be analyzed in terms of the $S = 1/2$ and $S = 3/2$ states corresponding to the antiferromagnetic and ferromagnetic alignment of the δ_π electrons (Figure 5). In addition, an $S = 5/2$ state involving metal centers with high-spin configurations (Figure 6) has to be considered.

As in the $[a_1e^3 \times a_1e^4]$ and $[a_1e^3 \times a_1^2e^3]$ modes, the same broken-symmetry configuration, corresponding to an $[(a_1)^2(e)^4(e)^1(a_1)^2]$ orbital occupancy, can describe both low-spin and high-spin cases because of the particular symmetry properties of the δ_π orbitals in the D_{3h} and C_{3v} point group.

Plots of the potential energy curves for the ($[a_1^2e^2 \times a_1^2e^3]$) broken-symmetry, $S = 1/2$, $S = 3/2$, and $S = 5/2$ states are shown in section (d) of Figure 7. The broken-symmetry and $S = 3/2$ curves are close or almost coincident at all metal−metal separations, with the global minimum occurring at an Fe−Fe bond length of 3.00−3.05 Å, whereas the $S = 1/2$ and $S = 5/2$ curves become important only at the shortest and longest Fe−Fe distances investigated, respectively.

3.2.2. General Analysis of the Potential Energy Curves. The potential energy curves for the states that are most relevant to determining the global minima of $[Fe_2Cl_9]^{2-}$, $[Ru_2Cl_9]^{2-}$, and $[Os_2Cl_9]^{2-}$ are collected in Figure 8. The quartet states from the $[a_1e^3 \times a_1^2e^3]$, $[a_1^2e^2 \times a_1e^4]$, and $[a_1^2e^2 \times a_1^2e^3]$ coupling modes are important in the analysis of the metal−metal interactions in all three d^4d^5 systems, but the most significant difference between $[Fe_2Cl_9]^{2-}$ and the heavier dimers lies in the fact that the $[a_1e^3 \times a_1e^4]$ $S = 1/2$ state plays a central role in the latter but not in the former, whereas the opposite observation applies to the $S = 9/2$ state in which the individual metal sites adopt high-spin configurations. This state is important for the Fe system but not the Ru and Os systems.

For $[Fe_2Cl_9]^{2-}$, the $S = 9/2$ state represents the lowest-lying potential energy curve at long metal−metal separations, but the quartet states are energetically more favorable at Fe−Fe distances shorter than 3.3 Å. The global minimum is predicted to occur at an Fe−Fe bond length of 2.88 Å and corresponds to the $S = 3/2$ state from the $[a_1e^3 \times a_1^2e^3]$ coupling mode. However, the predicted energetic difference between the $S = 9/2$ and $S = 3/2$ states is only 0.13 eV.

It is important to note that, in principle, the orbital degeneracy associated with the high-spin configuration of the d^4 Fe center in the $S = 9/2$ state could lead to Jahn−Teller distortions because of the fact that the degenerate

Table 5. Comparison of Calculated and Formal Properties for Odd- and Even-Electron Nb, Ta, Ru, and Os ($[M_2Cl_9]^{z-}$)Systems

metal	property	d^2d^2	d^1d^2	d^1d^1	metal	property	d^4d^4	d^4d^5	d^5d^5
Nb	M−M distance	2.69 Å	2.79 Å	2.87 Å	Ru	M−M distance	2.60 Å	2.65 Å	2.73 Å
	M−M formal bond order	$1.0\sigma + 1.0\delta_\pi$	$1.0\sigma + 0.5\delta_\pi$	1.0σ		M−M formal bond order	$1.0\sigma + 1.0\delta_\pi$	$1.0\sigma + 0.5\delta_\pi$	1.0σ
	M formal oxidation state	+3.0	+3.5	+4.0		M formal oxidation state	+4.0	+3.5	+3.0
	M Voronoi charge	+1.37	+1.48	+1.56		M Voronoi charge	+1.03	+0.98	+0.91
Ta	M−M distance	2.72 Å	2.82 Å	2.90 Å	Os	M−M distance	2.65 Å	2.71 Å	2.80 Å
	M−M formal bond order	$1.0\sigma + 1.0\delta_\pi$	$1.0\sigma + 0.5\delta_\pi$	1.0σ		M−M formal bond order	$1.0\sigma + 1.0\ \delta_\pi$	$1.0\sigma + 0.5\delta_\pi$	1.0σ
	M formal oxidation state	+3.0	+3.5	+4.0		M formal oxidation state	+4.0	+3.5	+3.0
	M Voronoi charge	+1.46	+1.57	+1.67		M Voronoi charge	+1.26	+1.20	+1.11

levels involved can be described as "modified e_g" orbitals. The possibility of observing these distortions has been explored by lowering the molecular symmetry to C_{2v} and C_s, thus removing the orbital degeneracy, but these calculations have revealed only minor structural and energetic differences.

In the case of $[Ru_2Cl_9]^{2-}$ and $[Os_2Cl_9]^{2-}$, the $[a_1e^3 \times a_1e^4]$ $S = 1/2$ state is favored at metal−metal separations shorter than 2.8−2.9 Å but shifts to higher energy at longer Ru−Ru or Os−Os distances, where the quartet states become increasingly stabilized. This doublet state represents the global minimum for the Os dimer at a bond length of 2.70 Å, but the calculations on the Ru dimer predict an energetic difference of only approximately 0.03 eV between the $[a_1e^3 \times a_1e^4]$ $S = 1/2$ and $[a_1e^3 \times a_1^2e^3]$ $S = 3/2$ states. Therefore, it is possible that this system may exhibit double-minima behavior (as previously found[11] for d^3d^4 $[Tc_2Cl_9]^{2-}$), with the corresponding Ru−Ru distances being 2.65 and 2.96 Å, respectively.

Experimental results based on a spectroelectrochemical study of $[Ru_2Cl_9]^{2-}$ have been reported[18] and interpreted as indicative of the presence of electron localization and no Ru−Ru bonding. It is therefore possible that the electrochemically generated species may correspond to the $[a_1e^3 \times a_1^2e^3]$ $S = 3/2$ state in which the δ_π electrons are decoupled (or ferromagnetically aligned) and the metal−metal bonding is formally represented by a σ interaction with a bond order of 0.5. In contrast, in the $[a_1e^3 \times a_1e^4]$ $S = 1/2$ state, the interaction between the metal centers is characterized by electron delocalization in a metal−metal bond with a formal bond order of 1.5, corresponding to $[1.0\sigma + 0.5\delta_\pi]$.

3.3. Comparison of Odd- and Even-Electron Systems. The results of calculations on odd-electron (mixed-valence d^1d^2 and d^4d^5) and even-electron (same-valence d^1d^1, d^2d^2, d^4d^4, and d^5d^5) $[M_2Cl_9]^{z-}$ species containing 4d and 5d elements are summarized in Table 5. These systems have, in general, a preference for electron delocalization and metal−metal bonding, and thus, all states used in the comparisons are characterized by formation of metal−metal bonds.

As found for the W and Re series in our previous study of the related d^2d^3 (Cr, Mo, W) and d^3d^4 (Mn, Tc, Re) dimers,[11] although the trends in computational (Voronoi) charges mirror those in formal metal oxidation states, the overall changes are rather small and suggest that electrostatic effects may play a relatively minor role. Similarly, examination of the $\sigma-\sigma^*$ and $\delta_\pi-\delta_\pi^*$ gaps suggests that both the σ and δ_π interactions should be important and that some metal−metal bond strengthening should occur as the formal metal oxidation states decrease from +4.0 to +3.0.

For all four systems described in Table 5, the shortening of the metal−metal distance as the configurations change, from d^1d^1 to d^2d^2 for $[Nb_2Cl_9]^{z-}$ and $[Ta_2Cl_9]^{z-}$ and from d^5d^5 to d^4d^4 for $[Ru_2Cl_9]^{z-}$ and $[Os_2Cl_9]^{z-}$, correlates with the increase in the formal metal−metal bond order from 1.0 to 2.0. In the Nb and Ta series, a small increase in the magnitude of the $\sigma-\sigma^*$ splittings is also observed, and as found for the (d^2d^2, d^2d^3, d^3d^3) $[W_2Cl_9]^{z-}$ series,[11] the changes in the bond order and strength of the σ interaction can be considered to act conjointly to cause the calculated metal−metal bond length to shorten by 0.18 Å between (d^1d^1) $[M_2Cl_9]^{1-}$ and (d^2d^2) $[M_2Cl_9]^{3-}$, with the metal−metal distance for the mixed-valence (d^1d^2) $[M_2Cl_9]^{2-}$ dimers lying approximately midway between those of the same-valence species.

A more significant variation in the magnitude of the $\sigma-\sigma^*$ splittings is predicted across the Ru and Os series, but the results for these systems are particularly different because the strengthening of the σ bonding, with the formal oxidation state decrease from +4.0 in (d^4d^4) $[M_2Cl_9]^{1-}$ to +3.0 in (d^5d^5) $[M_2Cl_9]^{3-}$, acts in opposition to the increase in metal−metal bond order. However, the latter factor appears to be more important in determining the changes in the metal−metal distances, which are predicted to shorten by 0.8−0.9 Å between (d^5d^5) $[M_2Cl_9]^{3-}$ and (d^4d^5) $[M_2Cl_9]^{2-}$ and by an additional 0.5−0.6 Å in (d^4d^4) $[M_2Cl_9]^{1-}$, as the formal bond order increases from 1.0, through 1.5, to 2.0. The opposite effects of oxidation state and bond order correlate with the fact that the overall change in the metal−metal bond length across the Ru and Os series is smaller than that found across the Nb and Ta series, namely, 0.13−0.15 Å compared to 0.18 Å.

In the case of the systems containing 3d elements, we have previously performed calculations[3,4] on (d^2d^2) $[V_2Cl_9]^{3-}$ and (d^5d^5) $[Fe_2Cl_9]^{3-}$, and these results can be compared with those reported in this work for (d^1d^2) $[V_2Cl_9]^{2-}$ and (d^4d^5) $[Fe_2Cl_9]^{2-}$, respectively. Unlike the 4d−4d and 5d−5d dimers, electron localization and weak coupling between the metal atoms tend to be favored in 3d−3d species.

The ground states for the d^1d^2 and d^2d^2 V dimers are predicted to be spin-quartet and spin-quintet states, respectively, with the calculated V−V distances lying in the 3.0−3.1 Å range. In both cases, a single electron occupies the a_1' orbital resulting in a formal σ bond order of 0.5, whereas

(18) Kennedy, B. J.; Heath, G. A.; Khoo, T. J. *Inorg. Chim. Acta* **1991**, *190*, 265.

the additional two or three δ_π electrons are ferromagnetically coupled and distributed over the e′ and e″ levels.

Calculations on (d^5d^5) $[Fe_2Cl_9]^{3-}$ predict that the ground state for this dimer corresponds to an $S = 5$ state, in which the individual metal sites adopt high-spin configurations, with an Fe−Fe distance of 3.43 Å. The analogous mixed-valence species is represented by the $S = 9$ state of (d^4d^5) $[Fe_2Cl_9]^{2-}$ which has a slightly shorter calculated Fe−Fe bond length of 3.39 Å. These systems formally do not contain metal−metal bonds, but the highest-occupied orbitals, which possess e″ symmetry (Figure 1), are metal−metal antibonding in nature, and the fact that an additional electron resides in these orbitals in (d^5d^5) $[Fe_2Cl_9]^{3-}$ relative to (d^4d^5) $[Fe_2Cl_9]^{2-}$ may be associated with the observed structural differences. In addition, the change in total molecular charge may also have an influence.

4. Conclusion

The electronic structures and metal−metal bonding in d^1d^2 (V, Nb, Ta) and d^4d^5 (Fe, Ru, Os) $[M_2Cl_9]^{2-}$ systems have been investigated by calculating the potential energy curves for various broken-symmetry and other spin states resulting from the d^1d^2 and d^4d^5 coupling modes. General similarities are observed in the behavior and properties of d^1d^2 and d^4d^5 systems, reflecting the electron−hole equivalence of the individual d^1-d^5 and d^2-d^4 configurations.

The global minima for (d^1d^2) $[Ta_2Cl_9]^{2-}$ and (d^4d^5) $[Os_2Cl_9]^{2-}$ correspond to spin-doublet states resulting from the $[a_1 \times a_1e]$ and $[a_1e^3 \times a_1e^4]$ coupling modes, respectively. This $S = 1/2$ state is characterized by delocalization of the metal-based electrons in relatively short metal−metal bonds with a formal bond order of 1.5 corresponding to $[1.0\sigma + 0.5\delta_\pi]$.

In contrast, the global minima of (d^1d^2) $[V_2Cl_9]^{2-}$ and (d^4d^5) $[Fe_2Cl_9]^{2-}$ are represented by spin-quartet states belonging to the $[e \times a_1e]$ and $[a_1e^3 \times a_1^2e^3]$ coupling modes, respectively. This $S = 3/2$ state results from the ferromagnetic coupling between δ_π electrons and thus predominantly involves electron localization and a weaker metal−metal interaction.

The (d^1d^2) $[Nb_2Cl_9]^{2-}$ and (d^4d^5) $[Ru_2Cl_9]^{2-}$ systems also show similarities, but while the metal−metal bonded spin-doublet state is clearly more stable than all of the other states in the case of $[Nb_2Cl_9]^{2-}$, the results obtained for $[Ru_2Cl_9]^{2-}$ indicate that both the spin-doublet and spin-quartet states should be energetically favored, and therefore, this dimer may exhibit double-minima behavior.

A comparison of the computational results across the (d^1d^1, d^1d^2, d^2d^2) $[Nb_2Cl_9]^{z-}$ and $[Ta_2Cl_9]^{z-}$ and (d^4d^4, d^4d^5, d^5d^5) $[Ru_2Cl_9]^{z-}$ and $[Os_2Cl_9]^{z-}$ series has revealed that the calculated shortening of the metal−metal distances, from d^1d^1 to d^2d^2 $[M_2Cl_9]^{z-}$ in the former and from d^5d^5 to d^4d^4 $[M_2Cl_9]^{z-}$ in the latter, appears to be primarily associated with a corresponding increase in the formal metal−metal bond order with the changes in the strength of σ bonding having a less significant influence.

Acknowledgment. Financial support from the Australian Research Council is gratefully acknowledged.

IC050175F